Polymer 50 (2009) 4837–4844

Contents lists available at ScienceDirect

Polymer

journal homepage: www.elsevier.com/locate/polymer

Interplay between nematic ordering and thermomechanical response in a side-chain liquid single crystal elastomer containing pendant azomesogen units

Valentina Domenici [a,b,*], Gabriela Ambrožič [c], Martin Čopič [d,a], Andrija Lebar [a], Irena Drevenšek-Olenik [d,a], Polona Umek [a], Boštjan Zalar [a,d], Blaž Zupančič [a], Majda Žigon [c]

[a] Department of Solid State Physics, J. Stefan Institute, Jamova 39, SI-1000 Ljubljana, Slovenia
[b] Dipartimento di Chimica e Chimica Industriale, Università degli studi di Pisa, via Risorgimento 35, 56126 Pisa, Italy
[c] National Institute of Chemistry, Hajdrihova 19, SI-1000 Ljubljana, Slovenia
[d] Department of Physics, University of Ljubljana, Jamova 39, SI-1000 Ljubljana, Slovenia

ARTICLE INFO

Article history:
Received 8 May 2009
Received in revised form
31 July 2009
Accepted 13 August 2009
Available online 19 August 2009

Keywords:
Liquid single crystal elastomer
Orientational order
Nuclear magnetic resonance

ABSTRACT

Photoactive materials based on azobenzene derivatives exhibit interesting properties related to the reversible photo-isomerisation between the *trans* and *cis* isomers of the azo-compound. In this work we report the preparation and physical–chemical characterization of Liquid Single Crystal Elastomers (LSCEs) containing azobenzene derivative side-chain mesogens as co-monomer. The interplay between the orientational ordering and mechanical response in the nematic phase is investigated by thermomechanical measurements as well as by deuteron NMR spectroscopy. We demonstrate that local nematic order can be reliably probed in azo-LSCEs using low molar mass deuterated cyanobiphenyl nematogen in low concentrations. No phase separation of the dopant is observed. The nematoelastic coupling $e_{av}(T) \propto S_{av}(T)$ between the effective sample deformation and average nematic order parameter is present over a wide temperature range even in the systems with relatively large heterogeneity of the nematic order and misaligned nematic domains.

1. Introduction

Liquid Crystal Elastomers (LCEs) are composed of self-organizing molecular units embedded in crosslinked polymer chains [1]. They possess properties characteristic of liquid crystals (high orientational order) and of polymer matrix. An important property of these systems is the so-called soft/semisoft elasticity, where the shape of the elastomer can be changed almost without any or with a very small energy cost by external strain, electric and magnetic fields, or by exposure to light [2–4] of visible- or near-visible-range (UV) wavelengths. Because of the ability to alter physical dimensions by a controlled change of the order parameter of the networked mesogen, liquid crystalline elastomers have huge application potential as artificial muscles, micropumps, microvalves and so on [5,6]. However, currently the biggest technological problem is how to actuate such materials. Thermomechanical actuation [7] is the best known example with high elongations, but is technologically impractical. Another type is actuation via Joule heating [8,9], where the elastomer is made conducting by adding conducting nanoparticles. Optomechanical approach [10] to actuation which relies on *trans* to *cis* photoisomerization of photoactive azo-dyes also bears a considerable application potential.

The introduction of azobenzene derivatives as dopants [11], chemically bonded pendant units [12], as well as photo-crosslinkers [13,14], in liquid crystalline polymers [15] and elastomers [10] has been widely explored in the recent decade with the purpose to enhance existing material properties or to enable new photo-induced effects. In particular, important improvements include photo-induced alignment [14] and related photo-induced optical anisotropy [16], light-induced nanopatterning and nanowriting [17] and various properties related to optical and holographic applications [18]. Another promising effect is photo-mechanical response [19], which is particularly large in LCE materials [10]. The use of azo-chromophores in liquid crystal elastomers is essential for the enhancement of the optomechanical response. At high doping concentrations the control of material shape, order, and dimensions can be attained by using relatively low power monochromatic light sources – for instance blue LEDs or blue laser sources in the mW power range [20]. Especially in the case of laser illumination, the

* Corresponding author. Dipartimento di Chimica e Chimica Industriale, Università degli studi di Pisa, via Risorgimento 35, 56126 Pisa, Italy. Tel.: +39 050 2219 266; fax: +39 050 2219 260.
E-mail address: valentin@dcci.unipi.it (V. Domenici).

0032-3861/$ – see front matter © 2009 Elsevier Ltd. All rights reserved.
doi:10.1016/j.polymer.2009.08.021

mesogenic nature of azo-additives is very important, since the alignment of the azomolecules provides for a much better coupling with polarized laser light [21,22]. These LCE materials are hence very suitable for fine manipulation and restructuring of the material with the use of tightly focused laser beams. They can also be patterned into various periodic structures by using the methods of optical holographic lithography [23]. In our work, new azobenzene doped LCEs have been prepared, for which recent investigations have shown that they can be used as holographic optical diffraction elements with broad range mechanically tunable periodicity [24]. The basic phenomenon in the background of this idea [24] is a very strong optomechanical response (i.e. change of optical properties by straining the material and vice versa) of our materials. In general, our materials are designed to achieve the following two main goals: (i) optical (re)structuring with low power monochromatic light sources and (ii) suitability for applications in new types of optomechanical elements for manipulation of monochromatic light beams. The latter can play an important role in optical communications and optical signal processing.

The efficiency and reproducibility of the peculiar properties of liquid crystalline elastomers [1], with or without the azo-chromophores, are strongly related to the interplay between the local orientational order and elastomechanical properties, i.e. the nematoelastic coupling. Rather little is known about the orientational ordering of polymer backbone, mesogen, comesogen, and crosslinker on the nanometric scale, particularly in view of ordering topology and its implications on the nematic ordering of the main network constituent, the mesogen/comesogen. The multicomponent character of the network and crosslinking constraints are anticipated to act as weak disorienting factors in the establishment of nematic order, resulting in a certain degree of local frustration, i.e. inhomogeneous nematic order and misaligned domains. It is this aspect of the local molecular ordering in LSCEs that we are primarily addressing in this work.

Thermomechanical response of liquid single crystal elastomers (LSCEs) is driven by the coupling between the orientational order of mesogenic molecular units and the ordering of polymer chain segments. The onset of nematic order of the mesogen results in a spontaneous change of the samples's geometry, i.e. in a contraction/extension of the linear dimension λ along the nematic director $\mathbf{n}$ and in an extension/contraction by $\sqrt{\lambda}$ in the two perpendicular directions [25]. Such behaviour can only be observed in samples with macroscopically broken isotropic symmetry and is not found in polydomain samples with isotropic average symmetry. Anisotropic networks are typically prepared by a two-stage "Finkelmann procedure" [26], which results in an anisotropic crosslinking of the network, leading to memorization of the domain state of the nematic phase even when the samples are kept in the high-temperature paranematic state for a long time. Due to this broken symmetry, LSCE samples can reach the ideal isotropic state only in the $T \to \infty$ limit. Theoretically, the interplay described above is modelled by a linear coupling term between the nematic order S and the mechanical deformation $e(T) = \lambda/\lambda(T \to \infty) - 1$ in the free energy functional, $f_{eS} = \alpha e S$, whereas the internal, symmetry breaking locked-in mechanical field g is taken into account by the linear term $f_g = -gS$ [27]. The high-temperature phase in LSCEs is not isotropic but rather paranematic, with a small, g-induced nematic order. The macroscopic mechanical response crucially depends on the local nematic order of mesogenic units as well as the alignment of nematic domains, therefore it is of paramount importance to precisely probe these microscopic properties. In ideal samples with spatially homogeneous chemical composition, the nematic order is uniform across the sample, resulting in a nematoelastic response $e(T) \propto S(T)$ [28]. In real samples, however, nematic order is spatially heterogeneous, $S = S(T, \mathbf{r})$, and so is the accompanying local mechanical deformation $e(T, \mathbf{r})$. A question then arises about the validity of the nematoelastic relation $e_{av}(T) \propto S_{av}(T)$ for the averaged quantities and, more specifically, what kind of averaging is implied in $e_{av}(T)$ and $S_{av}(T)$.

In this paper, we employ deuterated probe-doping NMR approach for the characterization of an azo-LSCE network, prepared from the scratch by synthesizing the basic constituents and by their subsequent polymerization into the network. We show that deuterated pentylcyanobiphenyl (5CB), embedded in the azo-LSCE network in small concentrations, sensitively probes the local nematic order of the LSCE network containing azomesogens. Furthermore, by comparing results of independent thermomechanical and deuteron NMR measurements, we prove that the nematoelastic relation $e_{av}(T) \propto S_{av}(T)$ is indeed satisfied in real samples with inhomogeneously distributed local nematic order parameter S.

2. Materials

2.1. Components of the LSCE network

Structures of azo-LSCE network basic building units are shown in Scheme 1. Benzoic acid phenyl ester-based mesogen (**2**) and the crosslinkers (**3**) are typical constituents of conventional side-chain LSCEs [26]. Azobenzene-based mesogen (**1**) is used to instill optomechanical response for potential use in tunable diffractive optical elements and related applications [24]. Components **1**–**3** were used as reagents in the hydrosilylation reaction with dimethylsiloxane polymer **4** also shown in Scheme 1. Syntheses of components **2** and **3** are described elsewhere [29,30].

All reagents and solvents were purchased from Sigma–Aldrich and used as received or purified using standard procedures.

2.2. Synthesis of (E)-4,4′-(hex-5-en-1-yloxy)-4′-methoxyazobenzene (**1**)

The synthesis of **1** was performed using different reagents and reaction conditions than described in the literature [31]. To

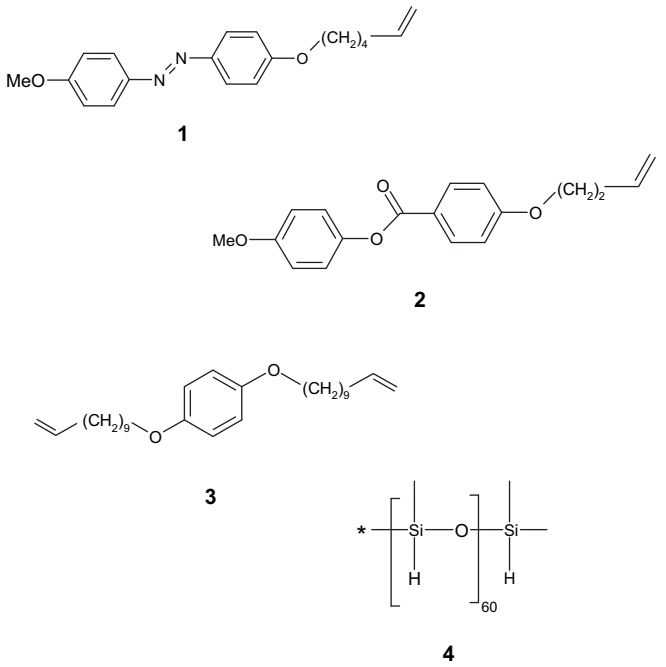

Scheme 1. Basic components for the preparation of the LSCE systems: mesogens **1**, **2**, flexible crosslinker **3**, and commercial polymeric chain hydroxymethyl-polysiloxane **4**.

a solution of (*E*)-4-hydroxyl-4′-methoxyazobenzene in dry DMF, five-fold molar excess of K_2CO_3 was added. After the addition of equimolar quantity of 6-bromo-2-hexene, the reaction mixture was stirred under reflux at 393 K. The reaction was monitored by TLC (SiO_2, $CHCl_3$:MeOH = 9.5:0.5). After the reaction was completed (8 h) the mixture was cooled down to room temperature. The crude product was precipitated by water addition. The precipitate was filtered, re-crystallized from ethanol, and vacuum dried. The overall yield for compound **1** is 95%. The mesomorphic behaviour was characterized by DSC. The following transition temperatures and enthalpies were found: $T_{C-LC} = 345$ K, $\Delta H_{C-LC} = 15.9$ J/g, $T_{LC-I} = 360$ K, and $\Delta H_{LC-I} = 99.1$ J/g. Here indices C, LC, and I denote crystal, liquid crystalline, and isotropic phase, respectively.

^{1}H NMR ($CDCl_3$-d_1, TMS): δ (ppm) = 7.87 (m, 4H, Ar), 6.99 (m, 4H, Ar), 5.84 (m, 1H, C*H*═CH_2), 5.02 (m, 2H, CH═C*H*$_2$), 4.04 (t, 2H, $J = 6.3$ Hz, –OC*H*$_2$–), 3.87 (s, 3H, –OCH_3), 2.14 (m, 2H, O–CH_2–C*H*$_2$–), 1.84 (m, 2H, –C*H*$_2$–CH═CH_2), 1.60 (m, 2H, O–$(CH_2)_2$–C*H*$_2$–).

^{13}C NMR ($CDCl_3$-d_1, TMS): δ (ppm) = 161.52, 161.14, 147.11, 146.95 (quaternary aromatic carbons), 138.44 (*C*H═CH_2), 114.81(CH═*C*H$_2$), 124.31, 124.00, 114.65, 114.15 (tertiary aromatic carbons), 66.07, 33.39, 28.64, 25.28 (4 *C*H$_2$), 55.53 (OCH_3). FT-IR (KBr): ν (cm^{-1}) = 1602 (st C═C), 1498 (st N═N). MS (EI): $m/z = 310$ (M^+). HR-MS: Calculated value for $C_{19}H_{22}N_2O_2$ (M^+): 310.168750; Experimental value: 310.168128. Mp: C 345 N 360 I (K).

2.3. Preparation of LSCE networks

The two-step "Finkelmann procedure" [26] has been followed in order to produce several monodomain side-chain LSCE films with various concentrations of azo-compound **1** as a co-monomeric unit. The composition of the six samples **E1/I**, **E1/II**, **E1/III**, **E1/IV**, **E1/V**, and **E1/VI** discussed in this paper is indicated in Table 1. The general scheme of preparation is summarized in the following.

The pre-polymerization mixture was prepared adding to 1 ml of anhydrous toluene: the poly(methylhydrosilane) (1 mmol), the crosslinker **3** (*c* %mmol), the mesogen **2** (*m* %mmol) and the azo-mesogen **1** (*a* %mmol). Note that $2c + m + a = 100$ %mmol. The Pt-catalyst is then added and the pre-polymerization mixture is filtered. The first step of the reaction is carried out in a special cylindrical form under centrifugation (spinning rate 4000–5000 rpm) at a temperature set between 338 K and 348 K, depending on the sample. After a period of time, calibrated for each LSCE system (typically 1–1.5 h, except for the **E1/I** which needed 2.5 h), a partially crosslinked, gel-like film network of dimensions 1×20 cm^2 and thickness of about 200 μm was removed from the form. The second step of reaction is performed at room temperature by mechanically loading the film with variable weights (1–3 g, depending on the crosslinker percentage) and then completing the crosslinking reaction in the oven at 338 K. During this second step, uniform uniaxial alignment of liquid crystal nematic domains is reached with the local director oriented along the direction of the weight-controlled external stress (vertical). Several monodomain stripes were made for all six LSCE films, respectively. Polydomain samples were also prepared without mechanically loading the gel films during the second crosslinking step. In all cases, the prepared films were swollen in toluene and dried in the oven at 320 K. This procedure was repeated two or three times, depending on the sample, in order to ensure that no unreacted mesogens or co-monomers were still present in the network. The absence of unreacted compounds was verified by ^{1}H NMR and FT-IR. The quality of the prepared systems was also checked by determining the swelling and unswelling anisotropy parameters [32] whose product was found to be close to 1, as in ideal reversible LSCE systems. The mesomorphic behaviour of the investigated LSCE samples, as determined by DSC, is reported in Table 2 and discussed in Section 4. The purity and thermal stability of the prepared azo-doped LSCE films are also evidenced by the excellent reproducibility of the DSC curves after first/second/third heating–cooling cycles. The nature of the mesophase of the prepared LSCE polydomain films was determined by polarized optical microscopy (not shown here). A schematic view of the composition of the LSCE systems is shown in Fig. 1.

Table 1
List of LSCE films investigated in the paper, showing the percentages of the basic components.

Label	Crosslinker **3** (%)	Azomesogen **1** (%)	Mesogen **2** (%)
E1/I	10	80	0
E1/II	5	9	81
E1/III	7.5	34	51
E1/IV	5	36	54
E1/V	7.5	5	80
E1/VI	7.5	1	84

2.4. Doping of LSCE networks with αd_2-5CB

In order to provide for selective deuteron NMR sensitivity, **E1/III** network was doped with pentylcyanobiphenyl (5CB) nematic liquid crystal ($T_{NI} \approx 308$ K), deuterated at the two α-positions of the alkyl chain. Doping was performed as follows. First the network was immersed in a 5CB-cyclohexane solution and then non-destructively swollen to about 400% of its initial volume V_0 by adding toluene in small steps. After soaking for a few hours at room temperature, the samples were de-swollen to V_0 by drying in the furnace at $T = 320$ K.

3. Experimental methods

3.1. Differential scanning calorimetry

Differential scanning calorimetry (DSC) analyses were carried out by a Perkin–Elmer DSC 7 calorimeter. The values of transition temperatures and corresponding enthalpies are given for the second heating and cooling cycle. Each sample was placed into a DSC heating cell at room temperature, cooled to 223 K and after 2 min heated to 413 K, maintained at this temperature for 2 min, cooled to 223 K, and reheated once again after 2 min. The heating and cooling rate was 10 K/min.

3.2. Chemical NMR spectroscopy

^{1}H and ^{13}C NMR spectra were recorded at 25 °C on a Varian VXR 300 spectrometer working at 300 MHz (^{1}H) and 75 MHz (^{13}C) using TMS as internal standard. $CDCl_3$-d_1 was used as a solvent.

Table 2
Temperatures (T), enthalpy (ΔH) and specific heat (C_p) of the phase transitions of the investigated E1 LSCEs at the second heating with a rate of 10 K/min. If not indicated otherwise, phase transitions are between the paranematic (PN) and nematic (N) phase and between the nematic and glass (G) phase.

Label	G	C_p (J/g K)	T (K)	N	ΔH (J/g)	T (K)	PN
E1/I	Crystal	8.74[a]	318.5	Smectic	1.28	345.1	•
E1/II	•	0.59	264.3	•	1.86	349.9	•
E1/III	•	0.53	261.2	•	1.05	345.2	•
E1/IV	•	0.19	263.3	•	2.53	349.9	•
E1/V	•	0.34	277.4	•	2.67	340.7	•
E1/VI	•	0.23	252.8	•	1.90	326.8	•

[a] ΔH (J/g).

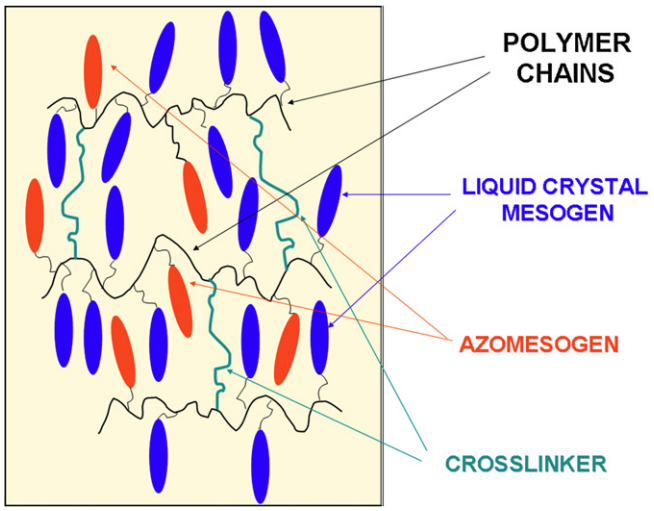

Fig. 1. Schematic picture of the molecular composition of the investigated LSCE systems.

3.3. IR spectroscopy

Infrared spectra were recorded on a Perkin–Elmer FT-IR 1725× spectrometer.

3.4. ^2H quadrupole-perturbed NMR spectroscopy

Deuteron NMR was performed with a home-built NMR spectrometer at the Larmor frequency $\nu_L(^2H) = 58.34$ MHz. Oxford Instruments continuous flow (nitrogen used as a cryogen) cryostat was used to control the temperature of the probe head with accuracy ±0.05 K. ^2H NMR spectra were recorded, either on cooling or on heating, by Quadrupolar Echo (QE) pulse sequence [33]. $t_{\pi/2} \approx 5$ μs pulses with QE time delay $\tau_{QE} = 30$ μs and relaxation delay $\tau_0 = 200$ ms were used. The number of scans was about 10,000. The measurements were performed on a sandwich-like sample prepared as described in Ref. [34], putting together 4 stripes of area 16 × 13 mm^2 with a macroscopic director aligned at a variable angle θ with respect to the external magnetic field.

3.5. Thermomechanical measurements

Thermomechanical measurements were performed in a home-built, nitrogen flow-controlled temperature cell made of glass. Ribbon-shaped samples with typical dimensions of 15 mm × 1.5 mm × 0.4 mm (length × width × thickness), except for the **E1**/**III** specimen with the width of ~3 mm, were freely suspended in the cell, with the upper end glued to a fixed metal frame, whereas a small metal weight with a mass $m \sim 200$ mg was attached to the lower end to minimize the movement of the sample in the gas flow. For all samples, the long edge matched the direction of nematic director **n**. m was selected low enough not to result in an external stress-induced sample elongation. Samples were marked at both ends with a fluorescent-coloured spots and the length of the sample, $\lambda(T)$, was determined as the distance between the spots from the photographs taken with a digital camera (Fig. 2).

4. Results and discussion

4.1. Thermotropic behaviour and chemical properties

The mesophase behaviour of the LSCE samples was determined by DSC. Fig. 3 shows the DSC curves obtained by heating and cooling a small portion of the polydomain LSCE sample **E1**/**V** with a flow rate of 10 K/min, as described in Section 3.1. Two phase transitions, specifically the nematic–paranematic and the glass-nematic one, can be clearly identified with a peak and a step, respectively, in the baseline of the two DSC curves (black arrows in Fig. 3). Similar curves were obtained for samples **E1**/**II**–**E1**/**VI**, whereas for **E1**/**I** the heating and cooling DSC curves are characterized by two peaks assigned to the smectic–paranematic and crystal–smectic phase transitions. In all six LSCE samples, the enthalpy of transition (ΔH) (for the nematic–paranematic, smectic–paranematic and crystal–smectic transitions, if observed) and the specific heat capacity of transition (C_p) (for the nematic-glass transition, if observed) were evaluated from the second heating DSC curve. Results are summarized in Table 2. The insertion of the azomesogen as a co-monomer in the LSCE network doesn't affect the sequence of mesophases if the relative concentration of the azomesogen is maintained below 36%. This is however not the case for the **E1**/**I** sample, where the conventional mesogen (**2**) was completely replaced by the azomesogen (**3**), reaching its maximum relative concentration (80%). Evidently, such a change in the composition of the basic chemical components of the LSCE network, which leads to a decrease of local flexibility, results in a disappearance of the nematic phase in favour of a more viscous

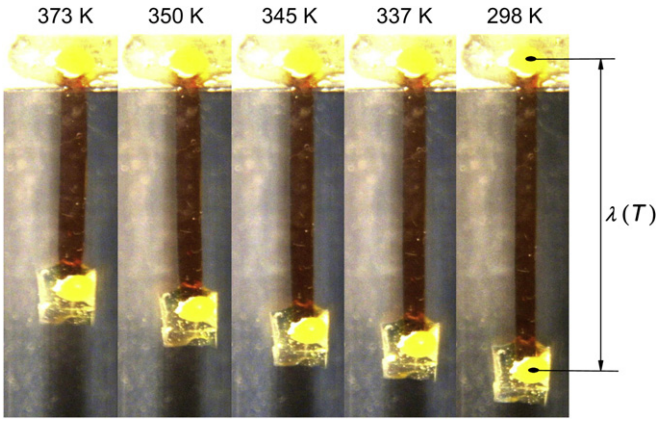

Fig. 2. Photographs of the experimental geometry of thermomechanical measurements, showing the T-dependent length of the **E1**/**III** specimen.

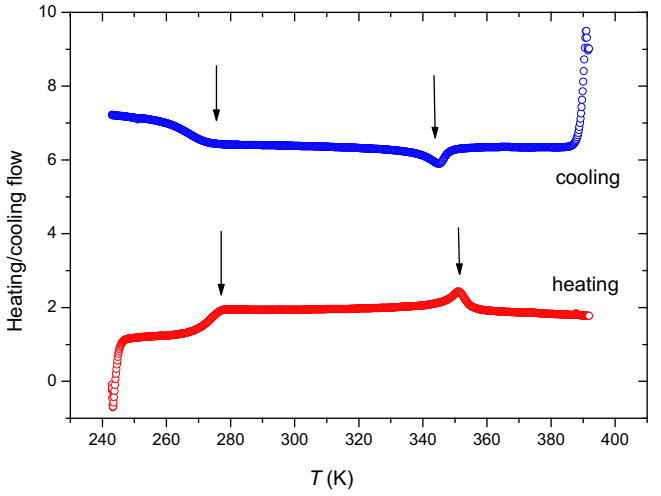

Fig. 3. DSC heating and cooling curves of the sample **E1**/**V**. The heating and cooling rate was 10 K/min.

and oriented phase, here identified as a smectic phase, based on the high Young modulus, as also commented below. Moreover, below 318.5 K, the system is already in the crystalline phase. On the contrary, samples **E1/II–E1/VI** are in the nematic phase at room temperature. No trends among these samples have been noticed in the temperature transitions with respect to the crosslinker-azomesogen relative concentrations (see Table 2).

A notable property of these new azo-LSCE films (**E1/II–E1/VI**), in view of technological applications, is the persistence of the nematic phase stable within a relatively large temperature range and in particular at room temperature, even at high concentrations of azomesogen.

4.2. Thermomechanical behaviour

The onset of the nematic order for **E1/II–E1/VI** is clearly visible in the temperature dependence of spontaneous mechanical deformation $e_{av}(T)$, determined from the $\lambda(T)$ measurements (Fig. 4). In accordance with the DSC results, no anomaly is seen, equivalently no nematic order is established, in the **E1/I** specimen. Although the identification of the exact nature of the smectic phase exhibited by the **E1/I** sample was not possible with our facilities, it is worth noting that the small thermomechanical response (with e less than 0.03) is not unusual in smectic LCEs [35] and LSCEs [36,37]. On the other hand, the stiffness of the sample prevented us from obtaining a well-aligned monodomain film and this may justify the behaviour reported in Fig. 4. Moreover, the high Young modulus of sample **E1/I** is not typical of nematic phases. This supports our conjecture on the smectic phase. For the other samples (**E1/II–E1/VI**), which are in the focus of our investigations, the nominal paranematic–nematic transition temperatures correspond to the ones determined from DSC. All monodomain LSCE samples revealed to be well oriented with relatively small differences in the value of the nematic–paranematic temperature transition. The maximum elongation of the LSCE is about 60% (**E1/V**) without using additional weights. This value is only slightly reduced when a azo-co-monomer is added in a percentage less than 36%.

With thermomechanical measurements, neither quantitative temperature profiles of the nematic order parameter $S_{av}(T)$ can be determined from the $e_{av}(T)$ curves due to unknown proportionality constant in the relation $e_{av}(T) \propto S_{av}(T)$, nor is it possible to compare the saturated values of S deep in the nematic phases among different samples since their respective proportionality constants can be rather different. This is why deuteron NMR, providing for a direct determination of S, has been employed.

4.3. Nematic order parameter

Temperature dependence of the deuteron NMR spectrum in αd_2-5CB-doped **E1/III** specimen is shown in Fig. 5. A gradual phase transition from the high-temperature paranematic phase into the low-temperature nematic phase is manifested through the appearance of the characteristic deuteron NMR doublet [38,39], split by

$$\Delta\nu(S,\theta) = 3/4\bar{\nu}_Q S\left(3\cos^2\theta - 1\right) \quad (1)$$

$\bar{\nu}_Q \approx 60$ kHz is the effective quadrupole coupling constant, averaged over fast reorientations about the 5CB long molecular axis. θ denotes the orientation of the sample, i.e. the angle between the external magnetic field and the nematic director **n**. What is notable is the small doublet splitting present even at the highest measured temperature points. The experimental $S(T)$ profile, obtained from the $\Delta\nu(T)$ experimental points, is given in Fig. 6a. The above-mentioned small nematic splitting is here discernible as a high-temperature $S(T)$ tail signifying the existence of paranematic order. It has been shown before [34,40] that it is originated by local mechanical fields, locked into the polymer network in order to preserve the monodomain nematic state.

4.4. Nematic and orientational disorder

The two deuteron NMR doublet lines (Fig. 5) possess a fairly large inhomogeneous line width. The temperature dependence of the full width at half maximum of the two respective doublet components, fwhm(T), exhibits a pronounced maximum (Fig. 6b) at the nominal temperature of the paranematic–nematic phase transition ($\sim$355 K for **E1/III**). Recently, this anomaly in fwhm(T) has been ascribed to heterogeneous S, i.e. to imperfect nematic

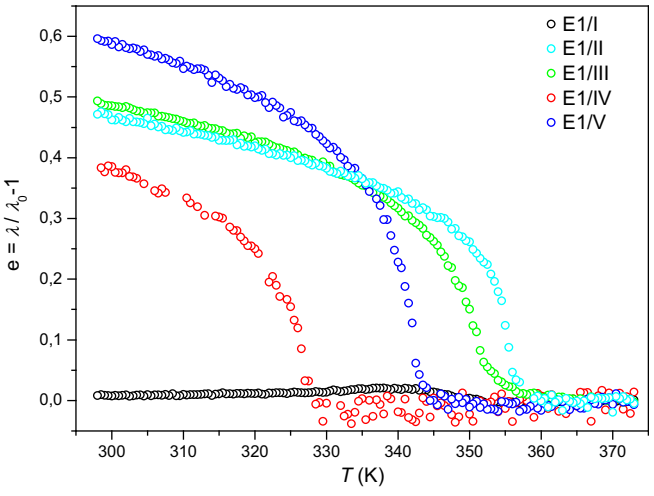

Fig. 4. Thermomechanical behaviour of several **E1** samples having the same type of azomesogen. The nematic phase disappears for high azomesogen concentrations.

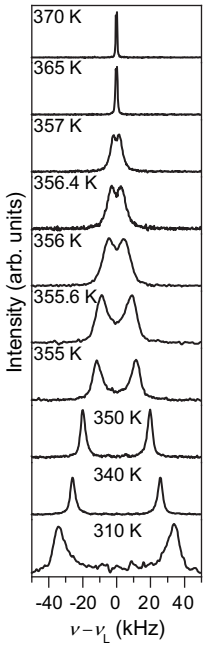

Fig. 5. Temperature dependence of the DNMR spectrum of αd_2-5CB-doped **E1/III** at the orientation $\theta = 0°$.

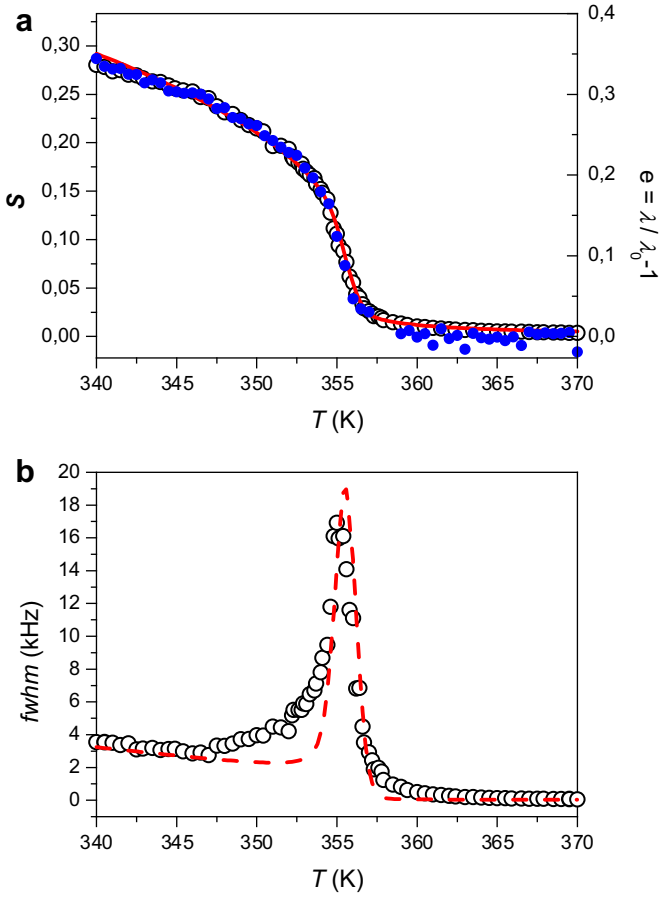

Fig. 6. (a) Comparison of temperature dependences of the nematic order parameter S (open black circles) and the mechanical deformation e (solid blue circles). Also shown is a fit (red solid line) to the theoretical model (see text); (b) Experimental (open circles) and theoretical (red dotted line) temperature dependences of the DNMR line width. All data are for the **E1**/**III** specimen. (For interpretation of the references to colour in this figure legend, the reader is referred to the web version of this article.)

order in real LSCE networks [34,41]. For such a case, disregarding the details on the distribution in S, Eq. (1) predicts fwhm to be roughly proportional to the width σ_S of the distribution of S, because of a linear relationship between $\Delta\nu$ and S. Consequently, the ratio fwhm/$\Delta\nu$ should be invariant to reorientations of the sample in the magnetic field, equivalently to variations of the angle θ. In order to check on that, we measured the angular dependences of the deuteron NMR spectra in both nematic and paranematic phases of **E1**/**III**. The spectra in Fig. 7 evidently demonstrate the monodomain character of the specimen, since $\Delta\nu(\theta)$ reproduces the angular dependence of Eq. (1). But contrary to assumptions made above, the ratio fwhm/$\Delta\nu$ falls short on being independent of θ. It reaches its maximum at about $\theta = 45°$. At this angle, the derivative of $3(\cos^2\theta - 1)$ with respect to θ is also maximal. This is reminiscent of uniaxial-like misalignment of nematic domains from their average orientation [34].

In spite of the substantial, experimentally verified disorder in S and director orientation, Fig. 6a demonstrates a remarkable match between the temperature profiles of the order parameter and the spontaneous mechanical deformation. Specifically, in an imperfect LSCE network, nematoelastic coupling $e(T) \propto S(T)$ seems to be well-satisfied for the average quantities $e_{\mathrm{av}}(T)$ and $S_{\mathrm{av}}(T)$. Here e_{av} is the macroscopic sample deformation, whereas $S_{\mathrm{av}}(T)$ is calculated from Eq. (1) with $\Delta\nu$ representing the frequency splitting of the maxima of the inhomogeneously broadened deuteron NMR doublet lines.

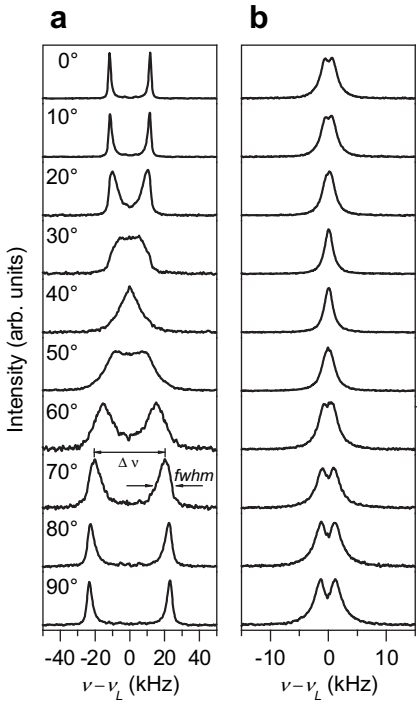

Fig. 7. Angular dependences of the DNMR spectrum of 5CB-doped **E1**/**III** in the nematic phase at $T = 345$ K (a) and in the paranematic phase $T = 357$ K (b).

4.5. Disorder and local mechanical fields

For a multicomponent system like LSCEs, it is straightforward to assume that the above described intrinsic disorder in nematic ordering and domain orientations comes from the local variations in the chemical composition. In particularly, the variation of the crosslinker concentration [41,42] across adjacent nematic domains gives rise to disorder-originated local mechanical fields $g_{\mathrm{dis}}(T, \mathbf{r})$, superimposed to intrinsic internal mechanical field $g_{\mathrm{int}}(\mathbf{r})$ as well as to eventual external stress g_{ext}, with a vanishing average over the sample, $\overline{g_{\mathrm{dis}}(T,\mathbf{r})} = g_{\mathrm{dis}}^{\mathrm{av}}(T) = 0$. Thermodynamically, each domain or cluster can then be regarded as conventional homogeneous nematoelastic system, exposed to local field $g(T, \mathbf{r}) = g_{\mathrm{dis}}(T, \mathbf{r}) + g_{\mathrm{int}}(\mathbf{r}) + g_{\mathrm{ext}}$. Its macroscopic thermomechanical response is then given by

$$e_{\mathrm{av}}(T) = \overline{e(T,\mathbf{r})} = \int w_e(e,T)\mathrm{d}e \propto \int w_S(S,T)\mathrm{d}S = \overline{S(T,\mathbf{r})} = S_{\mathrm{av}}(T). \quad (2)$$

It is the distribution $w_{\mathrm{e}}(e,T)$, equivalently $w_{\mathrm{S}}(S,T)$, which contains information on the mean value and dispersion of e and S. Although very little is known about the shape of these distributions in LSCEs, they are expected to be rather intricate, particularly in the systems with large, possibly glass-type disorder [43]. $e_{\mathrm{av}}(T)$ profile is easily measurable with a standard thermomechanical experiment, but this is not so in the case of its distribution function $w_{\mathrm{e}}(e,T)$. On the contrary, $w_{\mathrm{S}}(S,T)$, providing information equivalent to $w_{\mathrm{e}}(e,T)$ via the $e \propto S$ relationship, is readily accessible though a deuteron quadrupole-perturbed NMR experiment [34]. Unfortunately, selective deuteration of a specific constituent of the LSCE network, e.g. of benzoic acid phenyl ester mesogen **1** or methoxyazobenzene **2** (Scheme 1) is rather tedious, since considerable quantities of these compounds are needed to synthesize a well-aligned azo-LSCE sample, large enough to yield a satisfactory S/N level in a deuteron NMR experiment. Our approach, i.e. doping of LSCE networks with deuterated mesogenic probes, utilizes the fact that in a binary mixture of a side-chain liquid crystal polymer and low molar mass

nematogen, the nematic order parameters of the two mesogen species are alike, provided that the cross-interaction between the dissimilar mesogenic molecules has the same strength as the interaction between identical mesogenic molecules (“ideal mixing”) [44]. The compatibility of mesogens is reflected in the composition-dependence of the isotropic (I) to nematic (N) transition temperature, $T_{NI}(x)$. In the case of ideal mixing, T_{NI} varies linearly between the values corresponding to pure systems **A** and **B**, $T_{NI}(x)=(1-x)T_{NI}^{A}+xT_{NI}^{B}$, with x denoting the volume fraction of component **B**. Cyanobiphenyls were recently shown to mix well with conventional side-chain LSCEs [45], and their selectively deuterated (α-position in the alkyl chain) variants were successfully applied to the characterization of degree of nematic and domain orientation disorder [34,41]. The above considerations allowed for a safe use of deuterated probe-doping NMR approach for the characterization of thermodynamic behaviour of our system.

The continuous character of $S(T)$ (Fig. 6a) implies that the transition into the low-temperature nematic phase is supercritical, i.e. that the local mechanical fields g exceed the critical value g_c, resulting in a disappearance of the discontinuity in $S(T)$ [27]. In the alternative scenario, supported by the heterogeneous nature of our samples, the discontinuity is smeared due to distributed transition temperatures [40]. Only recently, deuteron NMR analytical approach, based on simultaneous measurements of the first and the second moments of the spectral lines, has been developed, which successfully resolves between the two scenarios [34,41]. The main steps of this procedure are as follows. In a weakly heterogeneous system, the second moment of the deuteron line is roughly proportional to the square of its line width (fwhm) of Fig. 6b. As reasoned in the preceding Section, the peak in fwhm(T) signifies heterogeneous nematic order. Specifically, from the maximum in fwhm(T) one can quantify the distribution $w_S(S)$, which determines the $S(T)$ profile, making it possible to resolve between the “supercritical” and “heterogeneous” scenario of the transition. In order to do that, we have performed theoretical modelling of $\lambda(T)$ by conventional Landau–de Gennes free energy functional by including the internal mechanical field term $-gS$ [41,42]. Gaussian distributed internal fields g of mean value g_0 and dispersion σ_g were assumed. Optimal fits are obtained with $T_{NI}=353$ K, $g_0/g_c\approx 1.1$, and $\sigma_g/g_c\approx 1.7$ (Fig. 6a and b). g_c is the critical field. According to our “distributed internal fields” model, the **E1**/**III** LSCE network behaves supercritically ($g_0>g_c$) in the thermodynamical sense [27,34]. Moreover, the dispersion σ_g of the internal fields is even larger than the mean internal field g_0, $\sigma_g/g_0\approx 1.5$, so that **E1**/**III** readily qualifies as quite heterogeneous. From the above statements it is obvious that an attempt at classifying our system as “supercritical” or “heterogeneous” is somewhat murky. In spite of the fact that it is supercritical on the average, below critical regions still exist in the sample. The $S(T)$ profile is continuous both due to supercritical diminishing of the discontinuity and due to heterogeneous smearing. We note that there are several ways of introducing heterogeneity into the above model, the most straightforward of them being the distribution in transition temperatures T_{NI} However, in the present case as well as in the previously studied systems [41], distributed internal fields result in a significantly better theoretical reproduction of experimental results than distributed transition temperatures.

5. Conclusions

We demonstrated that stable azo-LSCE networks can be prepared in a relatively wide range of crosslinker and azomesogen concentration. These networks are not ideal monodomains, they are rather imperfect, with non-ideally aligned nematic domains exhibiting heterogeneous nematic order. In spite of the imperfect structure, the networks exhibit an effective nematoelastic response $e_{av}(T)\propto S_{av}(T)$, with local deformation $e(\mathbf{r})$ replaced by effective macroscopic deformation $e_{av}(T)$ and local nematic order $S(\mathbf{r})$ replaced by the average nematic order $S_{av}(T)$. The proportionality between e and S persists in a wide temperature range, spanning from the high-temperature paranematic phase deeply into the nematic phase. We demonstrated that LSCE containing azomesogens in rather large amounts still retain similar thermomechanical and thermodynamic features as the standard LSCEs. The importance of this result is that it proves that doping with azo-chromophores profoundly enhances optomechanical response of the LCE materials without losing their usual strong coupling between the liquid crystalline ordering and mechanical properties. This means that standard LCE materials can be simply “upgraded” to become suitable for a new range of applications associated with manipulation and processing of optical signals. For instance, we observed that samples **E1**/**II**–**VI** display a substantial optomechanical response when *trans* to *cis* isomerisation is triggered by UV light with spatially periodic intensity profile. Their applicability as tunable holographic gratings is discussed in a separate publication [24].

Acknowledgements

Authors V. Domenici and B. Zalar thank the European Commission for the EIF Marie Curie Action project no. 039643. V. Domenici wish to thank Elke Stibal-Fisher for her precious suggestions for LSCE preparation.

References

[1] Warner M, Terentjev EM. Liquid crystal elastomers. Oxford: Oxford University Press; 2003.
[2] Yu Y, Nakano M, Ikeda T. Nature 2003;425:145.
[3] Ikeda T, Mamiya J, Yu Y. Angew Chem Int Ed 2007;46:506–28.
[4] Finkelmann H, Nishikawa E, Pereira GG, Warner M. Phys Rev Lett 2001;87:015501–4.
[5] Yu Y, Maeda T, Mamiya J, Ikeda T. Angew Chem Int Ed 2007;46:881–3.
[6] Madden JDW, Vandesteeg NA, Anquetil PA, Madden PGA, Takshi A, Pytel RZ, et al. Ocean Eng 2004;29:706–28.
[7] Brand HR, Finkelmann H. Physical properties of liquid crystalline elastomers. In: Demus D, Goodby J, Gray GW, Spiess HW, editors. Handbook of liquid crystals. Weinheim: Wiley VCH; 1998.
[8] Shenoy DK, Thomsen III D, Srinivasan A, Keller P, Ratna B. Sens Actuators A 2002;96:184–8.
[9] Chambers M, Zalar B, Remškar M, Žumer S, Finkelmann H. Appl Phys Lett 2006;89:243116–9.
[10] Camacho-Lopez M, Finkelmann H, Palffy-Muhoray P, Shelley M. Nat Mater 2004;3:307–10; Hogan PM, Tajbakhsh AR, Terentjev EM. Phys Rev E 2002;65:041720–9.
[11] Lee CR, Fu TL, Cheng KT, Mo TS, Fuh AYG. Phys Rev E 2004;69:031704–5.
[12] Gimenez R, Millaruelo M, Pinol M, Serrano JL, Vinuales A, Rosenhauer R, et al. Polymer 2005;46:9230–42.
[13] Takase H, Natansohn A, Rochon P. Polymer 2003;44:7345–51.
[14] Kawatsuki N, Uchida E. Polymer 2007;48:3066–73.
[15] Galli G, Chiellini E. Liq Cryst 2006;33:1297–301.
[16] Schab-Balcerzak E, Sapich B, Stumpe J. Polymer 2005;46:49–59.
[17] Galli G, Samaritani S, Chiellini E, Andreozzi L, Faetti M, Allegrini M, et al. Polymeric materials science engineering proceeding; 2006. p. 94.
[18] Shibaev VP, Kostromin SG. In: Shibaev VP, editor. Polymers as electroactive and photooptical media. Berlin: Springer; 1996.
[19] Barrett CJ, Mamiya JI, Yager KG, Ikeda T. Soft Matter 2007;3:1249–61.
[20] Lucchetti L, Di Fabrizio M, Francescangeli O, Simoni F. Opt Commun 2004;233:417–24.
[21] White TJ, Serak SV, Tabiryan NV, Vaia RA, Bunning TJ. J Mater Chem 2009;19:1080–5.
[22] Blinov LM, Cipparone G, Kozlovsky MV, Lazarev VV, Scaramuzza N. Opt Commun 2000;173:137–44.
[23] Harvey CLM, Terenjev EM. Eur Phys J E 2007;23:185–9.
[24] (a) Devetak M, Zupančič B, Lebar A, Umek P, Zalar B, Domenici V, et al. Phys Rev E, submitted for publication;
(b) Devetak M, Zupančič B, Lebar A, Umek P, Zalar B, Domenici V, et al. Poster P183, European congress of liquid crystals, Colmar, April 13–19, 2009.
[25] Tajbakhsh AR, Terentjev EM. Eur Phys J E 2001;6:181–8.
[26] Kupfer J, Finkelmann H. Macromol Chem Rapid Commun 1991;12:717–26.

[27] de Gennes PG. C R Acad Sci 1975;281:101–3.
[28] Clarke SM, Hotta A, Tajbakhsh AR, Terentjev EM. Phys Rev E 2001;64:061702–9.
[29] Ringsdorf H, Schmidt HW. Macromol Chem 1984;185:1327–34.
[30] Stewart D, Imrie CT. Polymer 1996;37:3419–25.
[31] Furniss BS, Hannaford AJ, Rogers V, Smith PWG, Tatchell AR. Vogel's textbook of practical organic chemistry. 5th ed. Harlow: Longman Scientific and Technical; 1989.
[32] Erman B, Baysal BM. Macromolecules 1985;18:1696–700.
[33] Luz Z, Meiboom S. J Chem Phys 1963;39:366–70.
[34] Lebar A, Kutnjak Z, Žumer S, Finkelmann H, Sánchez-Ferrer A, Zalar B. Phys Rev Lett 2005;94:197801–4.
[35] Ishige R, Tokita M, Naito Y, Zhang CY, Watanabe J. Macromolecules 2008; 41:2671–6.
[36] Nishikawa N, Finkelmann H. Macromol Chem Phys 1999;200:312–22.
[37] Kramer D, Finkelmann H. Macromol Rapid Commun 2007;28:2318–24.
[38] Doane JW. In: Owens FJ, Poole CP, Farach HA, editors. Magnetic resonance of phase transitions. New York: Academic Press; 1979 [chapter 4].
[39] Disch S, Schmidt C, Finkelmann H. Macromol Rapid Commun 1994;15:303–10.
[40] Selinger JV, Jeon HG, Ratna BR. Phys Rev Lett 2002;89:225701-01.
[41] Cordoyiannis G, Lebar A, Zalar B, Žumer S, Finkelmann H, Kutnjak Z. Phys Rev Lett 2007;99:197801–4.
[42] Cordoyiannis G, Lebar A, Rožič B, Zalar B, Kutnjak Z, Žumer S, et al. Macromolecules 2009;42:2069–73.
[43] Feio G, Figueirinhas JL, Tajbakhsh AR, Terentjev EM. Phys Rev B 2008;78: 020201(R)-04.
[44] Chiu H-W, Kyu T. J Chem Phys 1995;103:7471–81.
[45] Yusuf Y, Ono Y, Sumisaki Y, Cladis PE, Brand HR, Finkelmann H, et al. Phys Rev E 2004;69:021710–8.